

Detection of Dysplasia in Barrett's Esophagus With In Vivo Depth-Resolved Nuclear Morphology Measurements

NEIL G. TERRY,* YIZHENG ZHU,* MATTHEW T. RINEHART,* WILLIAM J. BROWN,*[‡] STEVEN C. GEBHART,*[‡] STEPHANIE BRIGHT,[§] ELIZABETH CARRETTA,[§] COURTNEY G. ZIEFLE,[§] MASOUD PANJEHPOUR,^{||} JOSEPH GALANKO,^{||} RYAN D. MADANICK,[§] EVAN S. DELLON,[§] DIMITRI TREMBATH,[#] ANA BENNETT,** JOHN R. GOLDBLUM,** BERGEIN F. OVERHOLT,^{||} JOHN T. WOOSLEY,[#] NICHOLAS J. SHAHEEN,[§] and ADAM WAX*

*Department of Biomedical Engineering, Duke University, Durham, North Carolina; [‡]Oncoscope, Inc, Durham, North Carolina; [§]Center for Esophageal Diseases and Swallowing, ^{||}Department of Medicine, and [#]Department of Pathology, University of North Carolina, Chapel Hill, North Carolina; ^{||}Thompson Cancer Survival Center, Knoxville, Tennessee; and **Department of Pathology, Cleveland Clinic, Cleveland, Ohio

BACKGROUND & AIMS: Patients with Barrett's esophagus (BE) show increased risk of developing esophageal adenocarcinoma and are routinely examined using upper endoscopy with biopsy to detect neoplastic changes. Angle-resolved low coherence interferometry (a/LCI) uses in vivo depth-resolved nuclear morphology measurements to detect dysplasia. We assessed the clinical utility of a/LCI in the endoscopic surveillance of patients with BE. **METHODS:** Consecutive patients undergoing routine surveillance upper endoscopy for BE were recruited at 2 endoscopy centers. A novel, endoscope-compatible a/LCI system measured the mean diameter and refractive index of cell nuclei in esophageal epithelium at 172 biopsy sites in 46 patients. At each site, an a/LCI measurement was correlated with a concurrent endoscopic biopsy specimen. Each biopsy specimen was assessed histologically and classified as normal, nondysplastic BE, indeterminate for dysplasia, low-grade dysplasia (LGD), or high-grade dysplasia (HGD). The a/LCI data from multiple depths were analyzed to evaluate its ability to differentiate dysplastic from nondysplastic tissue. **RESULTS:** Pathology characterized 5 of the scanned sites as HGD, 8 as LGD, 75 as nondysplastic BE, 70 as normal tissue types, and 14 as indeterminate for dysplasia. The a/LCI nuclear size measurements separated dysplastic from nondysplastic tissue at a statistically significant ($P < .001$) level for the tissue segment 200 to 300 μm beneath the surface with an accuracy of 86% (147/172). A receiver operator characteristic analysis indicated an area under the curve of 0.91, and an optimized decision point gave 100% (13/13) sensitivity and 84% (134/159) specificity. **CONCLUSIONS:** These preliminary data suggest a/LCI is accurate in detecting dysplasia in vivo in patients with BE.

Keywords: Barrett's Esophagus; Optical Techniques; Light Scattering.

Esophageal adenocarcinoma is rapidly increasing in incidence in the United States.¹ Barrett's esophagus (BE), a metaplastic transformation of the esophageal lining from squamous epithelium to a specialized columnar epithelium containing goblet cells, has long been recognized as a precursor lesion to esophageal adenocarcinoma.^{2,3} BE is believed to progress through stages of dysplasia before developing into esophageal adenocarcinoma. The incidence of adenocarcinoma in patients with BE increases with the degree of dysplasia from approximately 0.5% per year^{4,5} in nondysplastic BE to as high as 15% to 20% per year in subjects with high-grade dysplasia (HGD).^{6,7} Current techniques for endoscopic monitoring of the disease represent a large cost burden, the value of which has been called into question.⁸

The current procedure commonly used for monitoring tissue health in patients with BE consists of periodic endoscopic surveillance with systematic biopsies. Four-quadrant biopsy specimens are taken at 1- to 2-cm intervals along the entire segment of affected esophageal tissue. Surveillance procedures call for periodic examinations, with the frequency dictated by the degree of dysplasia observed.⁴ This approach has inherent limitations. Due to the need for sample processing, there is a time delay between endoscopy and diagnosis, requiring separate procedures for detection of dysplasia and treatment. In addition, diagnostic uncertainty often results due to the difficulties in analyzing the small, often histologically ambiguous tissue samples obtained during a standard biopsy, limiting interobserver agreement between pathologists.^{9,10} There is also a risk of misdiagnosis due to sampling error

Abbreviations used in this paper: a/LCI, angle-resolved low coherence interferometry; AUC, area under the curve; BE, Barrett's esophagus; CI, confidence interval; HGD, high-grade dysplasia; LGD, low-grade dysplasia; ROC, receiver operating characteristic.

© 2011 by the AGA Institute

0016-5085/\$36.00

doi:10.1053/j.gastro.2010.09.008

in the affected tissue because of the small surface area that can be examined using 4-quadrant biopsy techniques, estimated to be between 4% and 6% of the metaplastic epithelium.¹¹

Developments in interventional therapies, such as radiofrequency ablation,⁶ photodynamic therapy,¹² and cryotherapy,¹³ show great promise for management of BE, with the potential to reduce the risk of cancer in patients found to have dysplasia. The limitations of currently accepted methods for monitoring and evaluating the disease state of patients with BE, coupled with the benefit from early diagnosis of dysplasia, point to an unmet need for additional tools to improve detection of dysplasia.

One promising approach for improving detection of dysplasia is the use of optical biopsy techniques based on light scattering measurements. The dominant interaction between light and tissue is elastic scattering, where light is delivered in one direction and scattered in another without a change in energy (wavelength). By controlling the delivery and collection geometry, it is possible to collect backscattered light and analyze its characteristics to infer morphologic structure within tissues, such as the size and distribution of cell nuclei. Several optical biopsy technologies have been developed for use during endoscopic procedures, including light scattering spectroscopy,^{14,15} 4-dimensional elastic light scattering fingerprinting,¹⁶ endoscopic confocal microscopy,¹⁷ and fluorescence imaging.¹⁸⁻²¹

We report the application of a novel light scattering technique, angle-resolved low coherence interferometry (a/LCI), that analyzes the angular distribution of elastically scattered light to make depth-resolved measurements of both the size and index of refraction of cell nuclei as a means to evaluate dysplasia in the setting of BE. This technology was adapted for probe-based delivery through the instrument channel,²² and its operating characteristics were assessed in a clinical study.

Patients and Methods

Clinical Study Protocol

Fifty consecutively enrolled subjects undergoing routine endoscopic surveillance for BE at one of 2 tertiary centers specializing in the care of subjects with BE provided informed consent for this study. All subjects were receiving acid suppressive therapy with proton pump

Table 1. Patient Characteristics for the Population of Patients Scanned in This Study

Age (y)	38–86 (mean, 62; SD, 11.6)
Sex (M/F)	29/17
Previously detected dysplasia	10/46 (22%)
Previously detected adenocarcinoma	0/46 (0%)

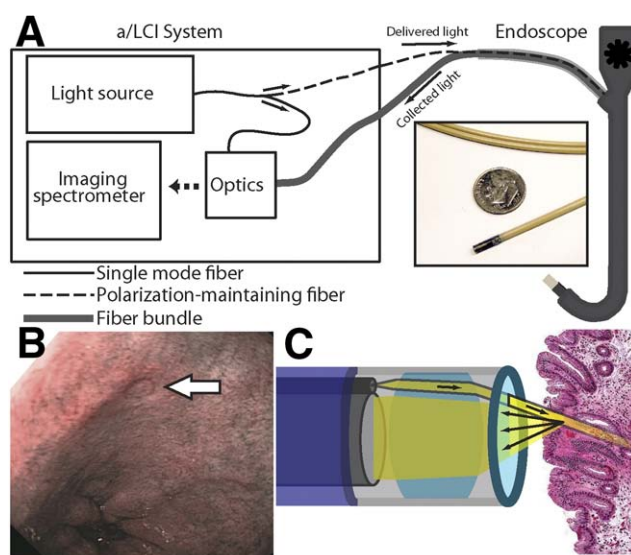


Figure 1. (A) High-level a/LCI system diagram. *Inset* shows scale of probe tip compared with a US dime. (B) Image showing the characteristic mark left by the a/LCI probe following deployment, indicated by the white arrow. (C) Detail of the a/LCI probe tip. Light is delivered as a collimated beam to the tissue. Scattered light is collected across the face of the fiber bundle for transport back to the a/LCI system.

inhibitors once to twice daily, and none had undergone previous ablative therapy or displayed evidence of esophagitis. Patients with a history of esophageal cancer or esophageal resection were excluded. The characteristics of the patient population for this study are shown in Table 1.

In each patient, images of 3 to 6 mucosal locations of columnar mucosa in the tubular esophagus were obtained using the a/LCI system (Figure 1) at random points. A matching histologic biopsy specimen was obtained at each imaged point. The protocol for acquisition of images and biopsy specimens was as follows. On selection of an imaging site, the endoscopist deployed the a/LCI fiber probe through the accessory channel and into the esophagus. The probe was brought into contact with the surface of the tissue and 10 to 30 data acquisitions of 25 milliseconds each were taken at each imaging location. Real-time analysis of image quality was performed in the room by a technician, who advised repositioning of the probe in the case of poor signal quality. Following data collection with the a/LCI system, the fiber probe was removed from the instrument channel, and biopsy forceps were deployed to collect a tissue biopsy specimen at precisely the same location. Guidance for localization of the physical biopsy specimen was facilitated by a clearly visible, but temporary, indentation left by an approximately 1-mm protruding rim on the surface of the a/LCI probe (white arrow in Figure 1B). The entire study consisted of 172 unique paired biopsy specimens, for which a total of 3397 data scans were acquired and analyzed.

The biopsy specimens collected from the scanned sites were fixed, sectioned, and stained with H&E, and each was analyzed by a pathologist at a central pathology laboratory with expertise in gastrointestinal pathology to assess the presence and degree of dysplasia. Pathologists were blinded to the results of the a/LCI scan. The biopsy specimens were classified as normal (squamous, gastric, squamocolumnar junction), nondysplastic BE, BE indeterminate for dysplasia, BE positive for low-grade dysplasia (LGD), and BE positive for HGD. If biopsy specimens at the squamocolumnar junction contained both squamous and gastric tissue, they were grouped with the “normal” tissue types because they do not contain goblet cells. Any biopsy specimen found to have dysplasia was confirmed by a second expert pathologist, with discrepancies resolved by consensus. The histologic assessments of dysplasia were compared with measurements taken by the a/LCI system to determine the ability of a/LCI to identify dysplasia. The study design was approved by the institutional review boards at the University of North Carolina at Chapel Hill and the Thompson Cancer Survival Center in Knoxville, Tennessee.

a/LCI

The a/LCI method is based on measuring the angular distribution of scattered light as a function of depth beneath the tissue surface. The scattered light from each tissue layer is analyzed to determine the mean size and average density of the cell nuclei in the probed area.^{23,24} The morphology of the cell nuclei is determined by comparison of the angular scattering data with the predictions of Mie theory, an analytical model of electromagnetic scattering by homogeneous spheres.^{25,26} Although this theory assumes a spherical nucleus, mathematical^{27,28} and experimental^{29,30} studies have shown that accurate structural measurements of spheroids can be made with this approach. Further, previous studies of neoplastic transformation in animal models have shown that this approximation provides high sensitivity and specificity for discriminating nondysplastic from dysplastic tissues.^{31–33} For the current study, the experimental data were analyzed by comparison with a database of Mie theory scattering solutions that describe the elastic light scattering patterns for a range of cell nuclei sizes and indices of refraction relative to the surrounding cytoplasm (representing nucleus density).

Depth resolution is achieved in a/LCI by using interferometry in a manner similar to that used in Fourier domain optical coherence tomography.³⁴ Light that has been scattered from the tissue is mixed with a reference light beam that has traveled a matched optical path, generating an interference pattern that appears as a spectral modulation in the detected signal. The spectrally resolved data are Fourier transformed to separate the scattered light by its path length within the tissue. The

depth resolution that is achieved by this technique is set by the bandwidth of the light delivered.

Endoscopic Fiber Probe

We developed a fiber-optic probe for clinical a/LCI operation that is compatible with the accessory channel of a standard endoscope.^{22,35} The probe is 230 cm in length, long enough to pass through the accessory channel of a 105-cm working distance gastroscope, and 2.5 mm in diameter, compatible with the instrument channel of most endoscopes. The fiber probe is encased in a plastic sheath for protection of the internal components, which also provides low friction to facilitate movement through the accessory channel. The distal end of the probe transmits light to the esophageal lumen via a polarization-maintaining optical fiber. To enable a/LCI measurements, the probe face is placed in contact with the tissue to provide a consistent geometrical interface. The incident light is formed into a collimated beam, approximately 0.4 mm in diameter, and delivered to the tissue at an oblique angle using a small lens incorporated in the probe tip, as shown in Figure 1C. This lens also serves to collect the backscattered light as a function of scattering angle. The 0.4-mm size of the beam represents the field of view probed by the a/LCI system in each data acquisition. The scattered light is relayed back to the a/LCI base unit via a 2.3-m-long imaging fiber bundle (Schott NA, Southbridge, MA), which is 1.1 mm in diameter and contains 18,000 optical fibers arranged in a parallel orientation relative to the delivery fiber.

Clinical a/LCI System

The a/LCI optical engine consists of a light source used to generate light for delivery to the tissue and an interferometer used to analyze the light returned from the tissue by the fiber probe (Figure 1A).²² The light source used by the a/LCI system is a superluminescent light-emitting diode (Superlum Ltd, Moscow, Russia) with a center wavelength of 832 nm and a bandwidth of 19 nm. The large bandwidth is required to achieve depth resolution. The superluminescent light-emitting diode output light is coupled into an optical fiber and split into reference and sample arms. The polarization of the light passed into the sample arm is controlled by an in-line polarizer before it is introduced into a polarization-maintaining fiber in the probe. The imaging fiber bundle in the probe returns the angular scattering pattern of light from the tissue to the optical engine. The light emerging from the proximal face of the fiber bundle is imaged onto the input slit of a spectrometer (SP 2150i; PI Acton, Acton, MA) after it is mixed with the path length-matched light from the reference fiber. The system is controlled by a laptop computer, which provides synchronized control of the delivery light and analyzes the detected signal in real time. The a/LCI systems allow for

subsecond data collection (25 milliseconds per image) and processing of the scattered light, which enables multiple a/LCI data points to be acquired without significantly increasing procedure time. Because of the short acquisition time, respiratory variation does not impact image quality.

Image Data Analysis

The data collected during the optical biopsies were processed using the following procedures. Each scan was normalized to account for the specific characteristics of the fiber probe used during the acquisition and then analyzed using the procedure described by Brown et al,²³ in which the angular scattering pattern contributed by the cell nuclei for each depth is isolated and compared with a predetermined database of scattering patterns, generated using Mie theory. The best fit for the detected signal from this database is selected using χ^2 analysis and is used to identify the nuclear size and index of refraction for each tissue site and subsurface location. Each analyzed point must pass 3 data quality checkpoints to confirm that a unique morphologic determination has been found, including signal strength, comparison with the next best size, and comparison with a null solution.²³ Scans with an inadequate signal for evaluation were discarded.

Each scan was analyzed in 50- μm depth increments and processed across the uppermost 500 μm of the tissue, yielding up to 10 measurements of nuclear size and index of refraction for each depth scan. For each scan, the surface of the tissue was identified from the depth-resolved data and the uppermost 300 μm of the tissue was segmented into three 100- μm segments for analysis by combining up to 2 measurements from each of the 50- μm depth increments. This depth range covers the expected thickness of the epithelium of the probed tissue. To ensure that sufficient tissue scattering was present to generate a meaningful result, scans of low amplitude (caused by normal esophageal motion) were rejected. To generate a consensus size and index of refraction measurement for each segment from an individual paired biopsy site, the results for all individual qualifying scans taken at the site were averaged to create a unique size measurement for that specific site. Data from each of the three 100- μm tissue layers were analyzed and compared independently with pathological diagnosis to determine if correlation with dysplastic state was possible at a statistically significant level.

Statistical Analysis

Statistical analyses were used to assess the association of dysplasia with morphologic nuclear characteristics after adjusting for other relevant factors. Specifically, repeated-measures logistic regression models were fit. For each model, the outcome variable was dichotomized as

dysplasia versus no dysplasia. The main predictor was the morphologic nuclear characteristic (nuclear density or nuclear diameter at a depth of 0–100 μm , 100–200 μm , and 200–300 μm , for a total of 6 models). Potential confounders to be adjusted for were age, sex, site, baseline diagnosis, and clinical diagnosis. A compound symmetric correlation matrix was used to account for the repeated measures within subjects, and diagnostics were performed to assess the fit of the model to the data. Each of the potential confounders was entered into a model with the nuclear characteristic, and those that proved statistically significant were included in the final model. *P* values associated with type I error rates of less than .05 were considered statistically significant in this study. Analyses were performed using SAS version 9.2 (SAS Institute, Inc, Cary, NC).

The relationship between sensitivity and specificity was determined through the development of a receiver operating characteristic (ROC) for the collected data. For this analysis, the presence of dysplasia was considered as a binary classifier and nuclear diameter was used as an evaluation characteristic. To evaluate the value of nuclear size as a predictive classifier, the area under the ROC curve (AUC) was calculated as a fraction of the maximum possible AUC.

Interobserver agreement between the a/LCI system and the independent pathologist was measured using the κ statistic.³⁶ The κ statistic provides a framework for evaluating the agreement between 2 independent observers of the same data. Agreement between observers can be assessed by determining a characteristic κ value between 1 (perfectly correlated) and -1 (anticorrelated). κ values less than zero were not observed in this study.

Results

Imaging Data

Forty-six patients were scanned with an a/LCI system. Four additional patients were enrolled but not scanned due to technical difficulties. Typical a/LCI data are shown in Figure 2. Figure 2A shows an angle-resolved depth scan, which is created by Fourier transforming the interferometric data collected by the spectrometer. Lighter shades of gray indicate higher intensity, which corresponds to higher levels of scattered light. Depth is indicated along the horizontal axis, with 0 μm corresponding to the interface between the tip of the fiber probe and the tissue surface. A total of 3397 scans were obtained but scans that yielded low intensity were excluded, resulting in the data set being reduced to 1866 scans, corresponding to a 45% rejection rate. No patients or biopsy specimens were discarded due to the rejection of individual scans. The collected data are summed across all angles and presented as an amplitude scan in Figure 2B. This represents scattered light as a function of

Figure 2. Typical a/LCI data. (A) Angle-resolved depth scan of light scattered from tissue. Lighter shades of gray indicate increased amount of scattered light. (B) Amplitude scan indicating depth increments used for processing. Tissue layers are labeled, and *gray bar* indicates basal layer. (C) Example angular scans for 3 tissue types pictured (*solid line*) with best-fit Mie theory solutions (*dashed line*) and size indicated.

depth with tissue layers indicated. For processing, angle-resolved data are analyzed by depth in 50- μm segments, as indicated in Figure 2B. For each depth segment, an angular profile of light scattered from the tissue is recovered. Once this angular profile has been filtered to remove noise, it is fit to the best Mie solution to determine its nuclear size and index of refraction. The creation of a single consensus size and index of refraction measurement for each depth at each biopsy site allowed the data to be reduced from 1866 data points to 516 morphologic measurements. Figure 2C shows 3 example angular profiles from tissue types with varied pathological diagnoses. These angular profiles (*solid line*) are shown along with the best-fit theory (*dashed line*) and the corresponding nuclear size.

Figure 3 shows a scatter plot of the mean nuclear size and average nuclear density for the basal epithelial layer (200- to 300- μm depth segment) for each paired biopsy specimen in the study. From these data, a simple decision

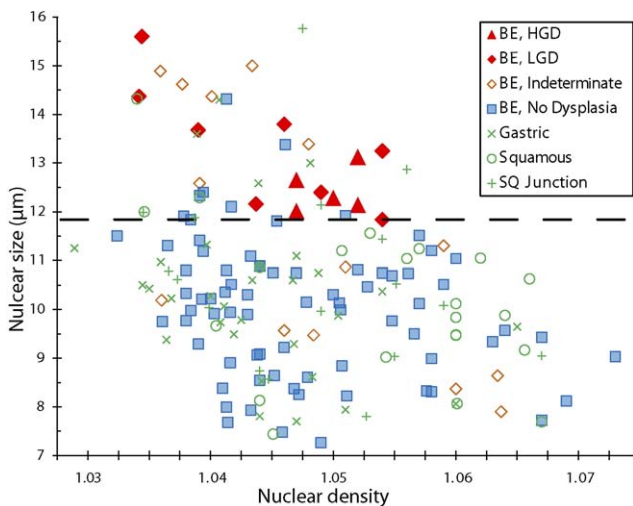


Figure 3. Scatter plot with each biopsy plotted as a function of its nuclear size and density, as measured by the a/LCI system, and categorized by its pathological diagnosis. *Dashed black line* indicates an optimized decision line between the 2 populations, resulting in 100% sensitivity and 84% specificity.

line can be drawn that well separates the samples diagnosed as normal tissue types from those diagnosed as dysplastic. Placing the decision line at 11.84 μm , as indicated in Figure 3 by the dashed black line, separates the 2 populations with maximum sensitivity and high specificity. Using this line, all 13 of the 13 biopsy specimens pathologically assessed as dysplastic (LGD and HGD combined) were also flagged by the a/LCI technique as dysplastic (100% sensitivity; 95% confidence interval [CI], 0.75–1.00). For nondysplastic tissue (normal, nondysplastic BE, and BE indeterminate for dysplasia), 134 of these 159 biopsy sites were correctly categorized by the a/LCI technique as nondysplastic (84% specificity; 95% CI, 0.78–0.90). Using the 11.84- μm cutoff, the a/LCI technique accurately classified dysplastic tissue and nondysplastic tissue at 147 of 172 biopsy sites (86% accuracy; 95% CI, 0.80–0.91). Use of this optimal decision line yielded a positive predictive value of 34% (13/38; 95% CI, 0.20–0.51) and a negative predictive value of 100% (134/134; 95% CI, 0.97 to 1.00). When biopsy specimens showing only squamous or gastric mucosa were disregarded and only biopsy specimens in which BE is present were considered, biopsy specimens positive for dysplasia were distinguished from indeterminate and nondysplastic BE with a sensitivity of 100% (13/13; 95% CI, 0.75–1.00) and a specificity of 85% (76/89; 95% CI, 0.76–0.92) using the same decision line.

ROC curves were generated using nuclear size as the differentiating variable to determine the relationship between sensitivity and specificity (Figure 4). Biopsy specimens identified in the pathology report as positive for dysplasia were characterized as diseased tissue ($n = 13$, true positives), whereas those identified as indeterminate for dysplasia, nondysplastic BE, squamous epithelium, gastric epithelium, or squamocolumnar junction were classified as nondysplastic tissue ($n = 159$, true negatives). Biopsy specimens identified as indeterminate for dysplasia ($n = 14$) were treated as nondysplastic in this analysis. The nuclear size data from the 200- to 300- μm layer showed the strongest distinction between dysplastic

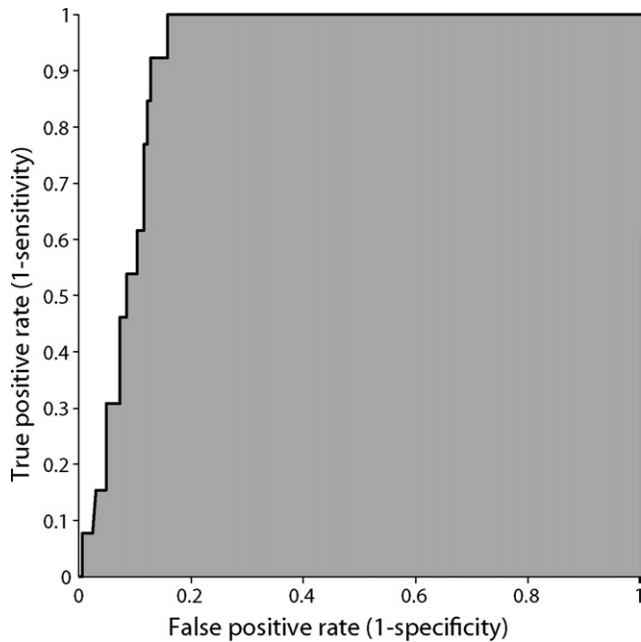


Figure 4. The ROC curve for the depth segment between 200 and 300 μm , indicating the relationship between sensitivity and specificity for varied decision lines using nuclear diameter as a discriminator. The gray area indicates the area under the curve (0.91). ROC curves for depth segments from 0 to 100 μm and from 100 to 200 μm (not shown) have an AUC of 0.58 and 0.52, respectively.

and nondysplastic tissue, with an AUC from the ROC curve of 0.91 (95% CI, 0.81–1.00). For the ROC for the data from the first and second 100- μm segments of tissue, the AUC values were 0.58 (95% CI, 0.42–0.75) and 0.52 (95% CI, 0.36–0.69), respectively, indicating that differentiation between dysplastic points and nondysplastic points at these shallower depths was indiscriminant. ROC analysis indicated that the optimal decision line to maximize both sensitivity and specificity fell at 11.99 μm . For this study, the decision line was placed at 11.84 μm , which maximized detection of dysplasia while sacrificing only a minimum of specificity.

In unadjusted models, nuclear diameters from 0 to 100 μm and 100 to 200 μm and nuclear density from 200 to 300 μm were not associated with a dysplastic diagnosis. Increases in nuclear diameter between 200 and 300 μm ($P = .0001$), in nuclear density between 0 and 100 μm ($P = .004$), and in nuclear density between 100 and 200 μm ($P = .01$) were associated with an increased likelihood of having dysplasia. Figure 5 shows the average nuclear diameter for all three 100- μm depth sections for each of the pathological categories (normal tissue, nondysplastic BE, and dysplasia). Increasing age predicted dysplasia in 5 of the 6 models, with a higher proportion of subjects recruited at Thompson Cancer Survival Center displaying dysplasia. As a result, age and site of enrollment were included in adjusted models as

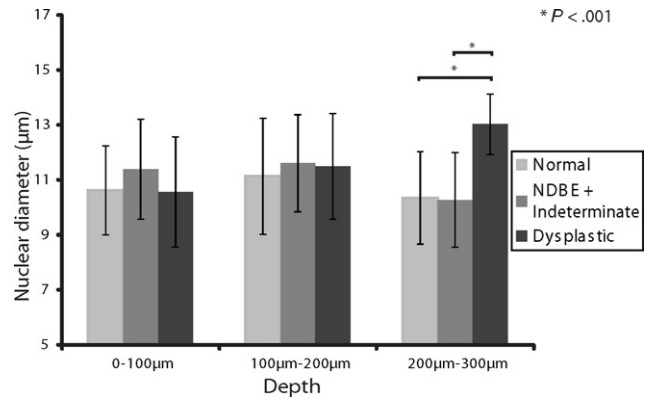


Figure 5. Nuclear size for each of the tissue layers segregated by pathological diagnosis.

appropriate. In the adjusted models, nuclear diameter between 0 and 100 μm and between 100 and 200 μm as well as nuclear density between 100 and 200 μm were not predictive of dysplasia. Nuclear diameter from the mucosal layer 200 to 300 μm beneath the surface ($P = .0001$) and nuclear density for the 0 to 100 μm deep layer ($P = .009$) were positively associated with having dysplasia, and nuclear density for the 200 to 300 μm deep layer ($P = .0009$) was negatively associated with dysplasia. Regression diagnostics showed a good fit of all constructed models. These results are summarized in Table 2.

Using the κ statistic to evaluate interobserver agreement,³⁶ a/LCI and histologic biopsy specimens agree at the “substantial” level for the distinction of dysplasia from nondysplastic BE ($\kappa = 0.60$) and for the distinction of dysplastic versus normal tissue ($\kappa = 0.60$). When the normal tissue and nondysplastic BE are grouped together as “nondysplastic,” the interobserver agreement is “moderate” ($\kappa = 0.45$).

Discussion

The data presented here show that a/LCI can detect a statistically significant enlargement of nuclear

Table 2. Summary of Statistical Analysis Used to Differentiate Dysplastic From Nondysplastic Tissue in Biopsy Populations Using Both Adjusted and Unadjusted Models

Nuclear characteristic	Adjusted variables	Unadjusted <i>P</i> value	Adjusted <i>P</i> value
Nuclear diameter (μm)			
0–100	Age, site	NS	NS
100–200	Age, site	NS	NS
200–300	Age, site	.0001	.0001
Nuclear density (μm)			
0–100	Age	.004	.009
100–200	Age, site	.01	NS
200–300	Age, site	NS	.0009

NS indicates that the specified characteristic did not differentiate dysplasia at a significant level ($P < .05$).

size in the basal layer of esophageal tissues found to be positive for dysplasia by histopathologic evaluation of biopsy specimens. Analysis of the nuclear morphology data for the 200- to 300- μm depth segment, which contains the basal layer of the epithelium, shows a correlation between increased nuclear size and the presence of dysplasia. This result is in agreement with previous a/LCI studies, in which nuclear size and index of refraction from the basal layer, contained in the third 100- μm layer, have been shown to be of particular diagnostic use.^{23,31} The high sensitivity and specificity shown in this study suggest that a/LCI may have utility in a clinical setting as a guide to target biopsies. Current biopsy techniques are inherently restricted to evaluating the limited amount of tissue that can be physically extracted. It has been shown that in up to 25% of cases where dysplasia has been previously identified, it is not found in follow-up surveillance procedures.^{6,37} This is likely due to the focal nature of the dysplastic changes, combined with sampling error associated with physical biopsy specimens. Due to the limited tissue coverage, traditional biopsy procedures would benefit from the use of an adjunct imaging modality with the ability to provide complementary information that can identify suspicious tissue regions. Upon showing adequate accuracy in detecting dysplastic tissue, this type of adjunct imaging modality could be used to improve and perhaps one day supplant histologic biopsies in a surveillance examination. Because optical biopsy allows sampling of more tissue sites in less time and without the expense and diagnostic limitations associated with histologic examination, it has significant potential to improve surveillance of BE tissues as an adjunct imaging modality. Further, the specific advantages of the a/LCI system, including rapid data acquisition and the potential for real-time analysis, could be exploited not only to increase surveillance coverage of at-risk tissues but also to potentially open up the possibility of therapeutic intervention within the same endoscopic session as the diagnostic procedure.

The sensitivity and specificity presented here are consistent with previous studies using this approach in which a/LCI has been shown to detect esophageal dysplasia in animal and human tissues. Dysplasia has been identified *in situ* in a rat carcinogenesis model with 100% sensitivity and 80% specificity ($n = 42$).³¹ A follow-up prospective study in this model showed 91% sensitivity and 97% specificity ($n = 82$) for predicting dysplasia.³³ An endoscopic a/LCI system was able to detect dysplasia with 100% sensitivity and 100% specificity ($n = 18$) in *ex vivo* human esophagus following resection of dysplastic BE tissue by esophagogastrectomy.³⁸ A second human study examining dysplasia in BE *in situ* was conducted in the pathology laboratory with a portable system, yielding 100% sensitivity and 78% specificity ($n = 15$).²³

Preliminary data are available for several other imaging modalities in detecting dysplasia in BE. Light-scattering spectroscopy has also been used to detect dysplasia in patients with BE ($n = 13$).¹⁰ This technique analyzes the spectral content of scattered light as a function of wavelength to measure the distribution of enlarged nuclei between the tissue surface and an estimated penetration depth of 100 to 200 μm . The approach was able to detect dysplasia (LGD and HGD combined) with sensitivity and specificity of 90% each. Georgakoudi et al used a trimodal spectroscopy technique that combines multiple spectroscopic measurements (fluorescence, reflectance, and light scattering spectroscopy) for the detection of dysplasia in patients with BE ($n = 16$).¹⁵ In this study, each of the aforementioned techniques was used to identify the presence of dysplasia. Intrinsic fluorescence spectroscopy and diffuse reflectance spectroscopy were both able to separate dysplastic from nondysplastic tissue with 79% sensitivity and 88% specificity. Light scattering spectroscopy separated the same sample population with 93% sensitivity and 96% specificity. When the results of all 3 techniques were combined, the resulting multimodal analysis was able to separate diseased tissue (LGD and HGD combined) from nondysplastic BE with 93% sensitivity and 100% specificity.¹⁵ A study conducted by Dunbar et al used a recently developed confocal endomicroscope to examine patients with BE ($n = 39$) to detect neoplasia.³⁹ Confocal endomicroscopy is capable of generating high-resolution images of the mucosal surface using an intravenously administered, exogenous contrast agent such as fluorescein. The images obtained in this study correlate with histology but require physician interpretation of the images to detect disease. By identifying the presence of irregular cells, the technique was able to predict BE-associated neoplasia with a sensitivity of 93% and a specificity of 98%. This technique, however, is typically limited to an image depth of less than 200 μm , which does not allow examination of the tissue depth that was found in this study to possess the most valuable diagnostic information.

In this study, the nuclear size data gathered from 0 to 100 μm and from 100 to 200 μm did not show diagnostic value. This may be due to confounding issues such as inflammation, which is expected to preferentially affect the surface of the esophagus, or may be due to the fact that basal nuclei are most informative with regard to the state of dysplasia. The differentiation observed for the nuclear size in the 200- to 300- μm depth segment of the epithelial tissue layer is significant. The ability of a/LCI to analyze this deep layer of tissue independently of the influence of the surface layers of the epithelium presents a unique capability not found in other endoscopic optical biopsy techniques used for the evaluation of BE.

The data from this study point to the potential clinical utility of a/LCI. The ability to provide quantitative depth-resolved measurements of nuclear morphology without the need for image interpretation or administration of a contrast agent is not found in current techniques. Alternative approaches, such as enhanced magnification endoscopy and endoscopic confocal microscopy, are able to provide detailed, high-resolution images of the epithelium, but these require histologic interpretation by the endoscopist.^{39,40} These techniques are also limited to investigation of the surface and topmost 100 μm of tissue, respectively, ignoring potentially relevant information regarding deeper tissue layers. Comprehensive imaging techniques, such as optical coherence tomography, can provide information about the entire epithelium but also require histologic interpretation of the images. In optical coherence tomography, discrimination of dysplastic tissue is further complicated by the fact that most optical coherence tomography systems do not possess the spatial resolution required for measurements of nuclear morphology.⁴¹

A shortcoming of the present study was the dichotomous nature of our outcome variable. Although classifying outcomes as either “dysplastic” or “nondysplastic” ignores the radically different clinical implications regarding degrees of dysplasia, it was useful to show proof of principle that the device could accurately discern between the two. It was also pragmatically necessary, given the small numbers of dysplastic biopsy specimens in the study. Further work will characterize the ability of the device to discriminate between grades of dysplasia. Another factor that might impact the findings of this study, and therefore limit the utility of a/LCI, is the high rate of variability between pathologists in the diagnosis of dysplasia in BE, as cited previously.^{9,10} Because the gold standard for this study was histological reading by expert pathologists, any errors in classification by the pathologists might turn a true positive into a false positive, or a true negative into a false negative, with respect to a/LCI imaging. Given the lack of other feasible gold standards for this study, as well as other studies that seek to validate new methods for detecting dysplasia, future work assessing the long-term outcomes of subjects found to be positive for dysplasia by a/LCI nuclear morphology measurements but negative for dysplasia by histology might illustrate the degree to which human error is impacting the present results.

In summary, this report presents the first clinical evaluation of a/LCI for detecting dysplasia in patients with BE. This in vivo study shows very strong agreement between pathological identification of dysplasia and nuclear enlargement, as measured using a/LCI, in the basal layer of epithelium. These results suggest

that a/LCI has promise as a complementary diagnostic tool for physicians in the surveillance of patients with BE for dysplasia. Development of real-time processing software would allow the endoscopist to identify suspicious tissue sites and collect biopsy specimens in a more targeted and perhaps more effective manner. The very high negative predictive value would allow an endoscopist to forgo biopsies at sites with a normal nuclear diameter while targeting biopsies to more suspicious regions. Any adjunct imaging tool that can show an improvement in the ability to identify dysplasia at an early stage increases the opportunity to implement an effective therapy. Further studies are planned to validate the findings presented here and to better define the ability of a/LCI as a tool for the endoscopic detection of dysplasia, both in the esophagus and at other organ sites.

References

1. Jemal A, Siegel R, Ward E, et al. Cancer statistics, 2009. *CA Cancer J Clin* 2009;59:225.
2. Spechler SJ, Goyal RK. The columnar-lined esophagus, intestinal metaplasia, and Norman Barrett. *Gastroenterology* 1996;110:614–621.
3. Spechler S. Barrett's esophagus. *GI Motility online* 2006; doi: 10.1038/gimo44.
4. Shaheen NJ, Richter JE. Barrett's oesophagus. *Lancet* 2009; 373:850–861.
5. Yousef F, Cardwell C, Cantwell M, et al. The incidence of esophageal cancer and high-grade dysplasia in Barrett's esophagus: a systematic review and meta-analysis. *Am J Epidemiol* 2008;168:237–249.
6. Shaheen NJ, Sharma P, Overholt BF, et al. Radiofrequency ablation in Barrett's esophagus with dysplasia. *N Engl J Med* 2009; 360:2277–2288.
7. Overholt BF, Lightdale CJ, Wang KK, et al. Photodynamic therapy with porfimer sodium for ablation of high-grade dysplasia in Barrett's esophagus: international, partially blinded, randomized phase III trial. *Gastrointest Endosc* 2005;62:488–498.
8. Barritt AST, Shaheen NJ. Should patients with Barrett's oesophagus be kept under surveillance? The case against. *Best Pract Res Clin Gastroenterol* 2008;22:741–750.
9. Downs-Kelly E, Mendelin JE, Bennett AE, et al. Poor interobserver agreement in the distinction of high-grade dysplasia and adenocarcinoma in pretreatment Barrett's esophagus biopsies. *Am J Gastroenterol* 2008;103:2333–2340.
10. Wallace MB, Perelman LT, Backman V, et al. Endoscopic detection of dysplasia in patients with Barrett's esophagus using light-scattering spectroscopy. *Gastroenterology* 2000;119:677–682.
11. Sharma P. Clinical practice. Barrett's esophagus. *N Engl J Med* 2009;361:2548–2556.
12. Overholt BF, Panjehpour M, Halberg DL. Photodynamic therapy for Barrett's esophagus with dysplasia and/or early stage carcinoma: long-term results. *Gastrointest Endosc* 2003;58:183–188.
13. Johnston MH, Eastone JA, Horwhat JD, et al. Cryoablation of Barrett's esophagus: a pilot study. *Gastrointest Endosc* 2005; 62:842–848.

14. Backman V, Gopal V, Kalashnikov M, et al. Measuring cellular structure at submicrometer scale with light scattering spectroscopy. *IEEE J Sel Top Quantum Electron* 2001;7:887–893.
15. Georgakoudi I, Jacobson BC, Van Dam J, et al. Fluorescence, reflectance, and light-scattering spectroscopy for evaluating dysplasia in patients with Barrett's esophagus. *Gastroenterology* 2001;120:1620–1629.
16. Roy HK, Liu Y, Wali RK, et al. Four-dimensional elastic light-scattering fingerprints as preneoplastic markers in the rat model of colon carcinogenesis. *Gastroenterology* 2004;126:1071–1081; discussion 948.
17. Polglase AL, McLaren WJ, Skinner SA, et al. A fluorescence confocal endomicroscope for in vivo microscopy of the upper- and the lower-GI tract. *Gastrointest Endosc* 2005;62:686–695.
18. Kara MA, Peters FP, Ten Kate FJ, et al. Endoscopic video autofluorescence imaging may improve the detection of early neoplasia in patients with Barrett's esophagus. *Gastrointest Endosc* 2005;61:679–685.
19. Fahmy M, Skacel M, Gramlich TL, et al. Chromosomal gains and genomic loss of p53 and p16 genes in Barrett's esophagus detected by fluorescence in situ hybridization of cytology specimens. *Mod Pathol* 2004;17:588–596.
20. Brankley SM, Wang KK, Harwood AR, et al. The development of a fluorescence in situ hybridization assay for the detection of dysplasia and adenocarcinoma in Barrett's esophagus. *J Mol Diagn* 2006;8:260–267.
21. Panjehpour M, Overholt BF, Vo-Dinh T, et al. Endoscopic fluorescence detection of high-grade dysplasia in Barrett's esophagus. *Gastroenterology* 1996;111:93–101.
22. Zhu Y, Terry NG, Woosley JT, et al. Design and validation of an angle-resolved low coherence interferometry fiber probe for in vivo clinical measurements of depth-resolved nuclear morphology. *J Biomed Opt* (in press).
23. Brown WJ, Pyhtila JW, Terry NG, et al. Review and recent development of angle-resolved low-coherence interferometry for detection of precancerous cells in human esophageal epithelium. *IEEE J Sel Top Quantum Electron* 2008;14:88–97.
24. Wax A, Yang CH, Backman V, et al. Cellular organization and substructure measured using angle-resolved low-coherence interferometry. *Biophys J* 2002;82:2256–2264.
25. Bohren CF, Huffman DR. Absorption and scattering of light by small particles. New York, NY; Wiley, 1983.
26. van de Hulst HC. Light scattering by small particles. New York, NY; Dover Publications, 1981.
27. Keener JD, Chalut KJ, Pyhtila JW, et al. Application of Mie theory to determine the structure of spheroidal scatterers in biological materials. *Opt Lett* 2007;32:1326–1328.
28. Chalut KJ, Giacomelli MG, Wax A. Application of Mie theory to assess structure of spheroidal scattering in backscattering geometries. *J Opt Soc Am A Opt Image Sci Vis* 2008;25:1866–1874.
29. Chalut KJ, Chen S, Finan JD, et al. Label-free, high-throughput measurements of dynamic changes in cell nuclei using angle-resolved low coherence interferometry. *Biophys J* 2008;94:4948–4956.
30. Amoozegar C, Giacomelli MG, Keener JD, et al. Experimental verification of T-matrix-based inverse light scattering analysis for assessing structure of spheroids as models of cell nuclei. *Appl Opt* 2009;48:D20–D25.
31. Wax A, Yang CH, Muller MG, et al. In situ detection of neoplastic transformation and chemopreventive effects in rat esophagus epithelium using angle-resolved low-coherence interferometry. *Cancer Res* 2003;63:3556–3559.
32. Chalut KJ, Kresty LA, Pyhtila JW, et al. In situ assessment of intraepithelial neoplasia in hamster trachea epithelium using angle-resolved low-coherence interferometry. *Cancer Epidemiol Biomarkers Prev* 2007;16:223–227.
33. Wax A, Pyhtila JW, Graf RN, et al. Prospective grading of neoplastic change in rat esophagus epithelium using angle-resolved low-coherence interferometry. *J Biomed Opt* 2005;10:051604.
34. Choma MA, Sarunic MV, Yang CH, et al. Sensitivity advantage of swept source and Fourier domain optical coherence tomography. *Opt Express* 2003;11:2183–2189.
35. Pyhtila JW, Boyer JD, Chalut KJ, et al. Fourier-domain angle-resolved low coherence interferometry through an endoscopic fiber bundle for light-scattering spectroscopy. *Opt Lett* 2006;31:772–774.
36. Landis JR, Koch GG. The measurement of observer agreement for categorical data. *Biometrics* 1977;33:159–174.
37. Conio M, Bianchi S, Lapertosa G, et al. Long-term endoscopic surveillance of patients with Barrett's esophagus. Incidence of dysplasia and adenocarcinoma: a prospective study. *Am J Gastroenterol* 2003;98:1931–1939.
38. Pyhtila JW, Chalut KJ, Boyer JD, et al. In situ detection of nuclear atypia in Barrett's esophagus by using angle-resolved low-coherence interferometry. *Gastrointest Endosc* 2007;65:487–491.
39. Dunbar KB, Okolo P III, Montgomery E, et al. Confocal laser endomicroscopy in Barrett's esophagus and endoscopically inapparent Barrett's neoplasia: a prospective, randomized, double-blind, controlled, crossover trial. *Gastrointest Endosc* 2009;70:645–654.
40. Curvers WL, Singh R, Song LM, et al. Endoscopic tri-modal imaging for detection of early neoplasia in Barrett's oesophagus: a multi-centre feasibility study using high-resolution endoscopy, autofluorescence imaging and narrow band imaging incorporated in one endoscopy system. *Gut* 2008;57:167–172.
41. Isenberg G, Sivak MV Jr, Chak A, et al. Accuracy of endoscopic optical coherence tomography in the detection of dysplasia in Barrett's esophagus: a prospective, double-blinded study. *Gastrointest Endosc* 2005;62:825–831.

Received February 26, 2010. Accepted September 9, 2010.

Reprint requests

Address requests for reprints to: Adam Wax, PhD, Box 90281, Durham, North Carolina 27708-0281. e-mail: a.wax@duke.edu; fax: (919) 684-4488.

Acknowledgments

N.J.S. and A.W. were equally-contributing senior authors on this work.

Conflicts of interest

The authors disclose the following: Dr Wax and Dr Brown have a financial interest in Oncoscope, Inc, the company that holds proprietary rights to the technology described in this study. Dr Gebhart and Mr Terry are consultants for Oncoscope, Inc. Dr Goldblum, Dr Overholt, and Dr Shaheen receive research support from Oncoscope, Inc. Dr Zhu, Mr Rinehart, Ms Bright, Ms Carretta, Ms Zieffle, Dr Panjehpour, Dr Galanko, Dr Madanick, Dr Dellon, Dr Trembath, Dr Bennett, and Dr Woosley disclose no conflicts.

Funding

Supported in part by the National Institutes of Health (National Cancer Institute R33-CA109907; DK 034987 and DK 056350), the National Science Foundation (BES 03-48204), a grant from the Coulter Foundation, and funding by Oncoscope, Inc, through a National Institutes of Health Small Business Innovative Research Phase II Grant.